RSC Advances

PAPER

View Article Online
View Journal | View Issue

CrossMark click for updates

Cite this: *RSC Adv.*, 2015, **5**, 90797

Mesoporous silica supported bimetallic Pd/Fe for enhanced dechlorination of tetrachloroethylene†

Ruey-an Doong,*[ab] Sandip Saha,[a] Cheng-hsien Lee[b] and Hong-ping Lin[c]

In this study, mesoporous silica (SiO_2) microspheres were hydrothermally synthesized in the presence of gelatin for the immobilization of bimetallic Pd/Fe nanoparticles (Pd–Fe/SiO_2) to enhance the dechlorination efficiency and dechlorination rate of tetrachloroethylene (PCE) under anoxic conditions. Scanning electron microscopy images and elemental mapping showed that the distribution of nanoscale zerovalent iron (NZVI, Fe) on SiO_2 was uniform and the density of Fe increased as the iron loading increased from 10 to 50 wt%. The optimized 30 wt% Fe/SiO_2 particles were used to fabricate Pd–Fe/SiO_2 microspheres by the electrochemical reduction of Pd ions to Pd^0 for the enhanced dechlorination of PCE under anoxic conditions. The dechlorination efficiency and rate of PCE by Fe/SiO_2 was significantly enhanced in the presence of 0.5–3 wt% Pd and the pseudo-first-order rate constant (k_{obs}) for PCE dechlorination by the mesoporous Pd–Fe/SiO_2 microspheres increased by 2–3 orders of magnitude when compared with that of Fe/SiO_2 alone. Ethane was found as the only end product with a carbon mass balance of 95–100%, showing that hydrodechlorination was the main reaction mechanism for PCE dechlorination by the Pd–Fe/SiO_2 microspheres. Column experiments showed the good mobility and permeability of the mesoporous Pd–Fe/SiO_2 microspheres when compared with that of pure NZVI alone. The results obtained in this study clearly show that the immobilization of bimetallic Pd–Fe nanoparticles on the mesoporous SiO_2 microspheres not only increases the reactivity for the dechlorination of PCE but also enhances the mobility and permeability for *in situ* remediation of chlorinated hydrocarbons in porous media.

Received 29th July 2015
Accepted 9th October 2015

DOI: 10.1039/c5ra15070a

www.rsc.org/advances

Published on 09 October 2015. Downloaded by Gazi Universitesi on 09/03/2016 01:28:36.

1. Introduction

The contamination of porous media such as soils and groundwater by dense non-aqueous phase liquids (DNAPLs) is becoming a serious environmental issue. DNAPLs such as tetrachloroethylene (PCE) and trichloroethylene (TCE) have been extensively used as cleaning solvents, aerosol propellants and refrigerants, and are released into aquatic environments as the priority pollutants in both surface water and groundwater.[1–3] These chemicals are possible carcinogens which pose a serious health concern to human beings because of their toxic and mutagenic behaviour.[4,5] Therefore, there is an urgent need for the development of an effective strategy for the removal of chlorinated hydrocarbons in contaminated aquifers.

Several technologies have been developed for the detection[6] and dechlorination of chlorinated hydrocarbons.[7–10] Permeable reactive barriers (PRBs) packed with zerovalent metals have been demonstrated to be an effective method for the removal of organic and inorganic pollutants under anoxic conditions.[11–13] Various laboratory-scale and field applications have found that nanoscale zerovalent iron (NZVI) and bimetallic iron-based nanoparticles including Fe/Pd and Fe/Ni can transform the chlorinated compounds into less-chlorinated homologues and non-chlorinated end products through reductive dechlorination and hydrodechlorination.[14–18] Several studies have shown that chlorinated hydrocarbons can be rapidly dechlorinated into non-chlorinated hydrocarbons by using nanoscale bimetallic Pd/Fe particles.[18,19] However, the aggregation of NZVI decreases the dechlorination efficiency and dechlorination rate of chlorinated compounds. Several studies have demonstrated the effectiveness of using a stabilizer or support to homogeneously disperse NZVI nanoparticles to enhance their stability and mobility.[20–28] Various organic polymers including carboxymethyl cellulose, polyacrylic acid (PAA) and electrospun PAA/polyvinyl alcohol nanofibers have been used to immobilize Pd/Fe for enhanced dechlorination efficiency and dechlorination rate of chlorinated compounds.[22,23] In addition, the organic polymer-immobilized iron-based nanoparticles have high

[a]*Institute of Environmental Engineering, National Chiao Tung University, Hsinchu, 30010, Taiwan. E-mail: radoong@nctu.edu.tw*

[b]*Department of Biomedical Engineering and Environmental Sciences, National Tsing Hua University, Hsinchu, 30013, Taiwan*

[c]*Department of Chemistry, National Cheng Kung University, Tainan, 700, Taiwan*

† Electronic supplementary information (ESI) available: TEM images and surface areas of mesoporous SiO_2; XRD patterns, adsorption and dechlorination of PCE by Fe/SiO_2; TEM images, deconvolution of XPS spectra and column experiments of Pd–Fe/SiO_2. See DOI: 10.1039/c5ra15070a

Published on 09 October 2015. Downloaded by Gazi Universitesi on 09/03/2016 01:28:36.

mobility to facilitate the nanoparticles' transport through soil columns.[24,25]

Another strategy for increasing the stability and reactivity of nanoparticles is the immobilization on supports such as membranes and carbon materials.[26–31] Parshetti and Doong[28] have immobilized bimetallic Ni/Fe nanoparticles in PVDF and nylon 66 membranes in the presence of polyethylene glycol for the dechlorination of TCE and found that the immobilization of the Fe/Ni nanoparticles in the hydrophilic membrane can retain the longevity and high reactivity of the nanoparticles towards TCE dechlorination. In addition, Su *et al.* used activated carbon-supported zerovalent iron (ZVI/AC) for the adsorption and dechlorination of TCE.[27] The rate constant for TCE dechlorination by ZVI/AC was 7 times higher than that of AC only. More recently, silica has been used as a support to maintain the reactivity and stability of iron-based nanoparticles.[32–34] The use of mesoporous SiO_2 microspheres as the support has several advantages including the prevention of NZVI agglomeration, environmental friendliness and increased reactivity and stability. Ensie and Samad have immobilized NZVI onto a SiO_2@FeOOH core using a reduction method to remove nitrate from drinking water and found that greater than 99% of the nitrate could be removed by the nano SiO_2@FeOOH@Fe core–shell material at pH 3.[34] In addition, Xie *et al.* compared four different iron-based nanoparticles for the dechlorination of polybrominated diphenyl ethers.[32] The results showed that the core–shell type SiO_2@FeOOH@Fe materials had higher usability and stability and a low Fe^{2+} leaching rate when compared to the other iron-based materials. It is noteworthy that a mesoporous SiO_2 microsphere is stable, environmentally friendly and can be transported with water in porous media. However, the use of mesoporous SiO_2 microspheres as a support for bimetallic Pd/Fe nanoparticles for the dechlorination of chlorinated hydrocarbons has received less attention. In addition, little information is available on the characterization and dechlorination efficiency of bimetallic Pd–Fe nanoparticles on mesoporous silica.

In this work, bimetallic Pd/Fe nanoparticles were immobilized onto mesoporous SiO_2 microspheres for PCE dechlorination under anoxic conditions. The mesoporous SiO_2 microspheres were hydrothermally fabricated in the presence of gelatin and then the bimetallic Pd/Fe nanoparticles were immobilized onto the surface of the mesoporous SiO_2. The properties of the microstructures of the Pd–Fe/SiO_2 microspheres including morphology, specific surface area, pore texture, and chemical species were characterized. The effect of the Fe and Pd loadings on the dechlorination efficiency and dechlorination rate of PCE was optimized. In addition, the longevity and stability of the mesoporous Pd–Fe/SiO_2 microspheres were investigated.

2. Materials and methods

2.1. Reagents

The chlorinated hydrocarbons including PCE and TCE (99.8%, GC grade) used in this study were purchased from Merck Co. (Darmstadt, Germany). Palladium acetate ($Pd(CH_3CO_2)_2$, 98%) was obtained from Fluka Co. (Tokyo, Japan). HEPES (*N*-[2-hydroxyethyl] piperazine-*N*′-[2-ethanesulfonic acid]) ($C_8H_{18}N_2O_4S$) and ferrous sulfate-7-hydrate ($FeSO_4 \cdot 7H_2O$) were purchased from Sigma Co. (St. Louis, MI). All other reagents were of analytical grade and were used as received without further treatment. In addition, deoxygenated water was prepared by vacuuming well-mixed deionized bidistilled water (18.3 MΩ cm, Millipore Co.) in serum bottles for 20 min and then purging with nitrogen for 5.0 min at 12.5 psi. The above procedure was repeated several times to remove the oxygen in the solutions.[9]

2.2. Synthesis of mesoporous silica

A stock solution of silicate was obtained upon mixing 20 g of sodium silicate, 250 mL of deionized bidistilled water and 250 mL of 0.1 M H_2SO_4 solution at 40 °C. The final pH of the solutions was then adjusted to 5. The fresh gelatine solution, prepared by adding 10 g of gelatin into 125 mL of water at 40 °C, was poured directly to the acidic solution of sodium silicate and stirred for several minutes. The solutions were hydrothermally treated at 100 °C for 1 d to form mesoporous silica. After cooling down to room temperature, the products were harvested by filtration, washed with water, dried in air and calcined at 550 °C.

2.3. Immobilization of Pd–Fe nanoparticles onto mesoporous silica

Fe/SiO_2 was synthesized by dispersing 0.3 g of mesoporous silica microspheres in 100 mL of bidistilled deionized water. 0.3 g of $FeSO_4 \cdot 7H_2O$ was added into the mesoporous SiO_2 solution and the Fe/SiO_2 microspheres were synthesized by the dropwise addition of 50 mL of 0.2 M ice-bathed $NaBH_4$ solution to reduce the ferrous ions into NZVI at pH 4 under stirring conditions. The mesoporous Fe/SiO_2 microspheres were collected by centrifugation at 14 000 rpm for 10 min and then dried in N_2. In addition, the bimetallic Pd–Fe/SiO_2 microspheres were fabricated using an electrochemical reduction method by the addition of deoxygenated 0.1–3 wt% $Pd(CH_3COO)_2$ solutions into the Fe/SiO_2 solutions under anoxic conditions. The Pd concentration in the Pd–Fe/SiO_2 microspheres was also examined by inductively coupled plasma-mass spectrometry (ICP-MS, Agilent 7500ce). The measured Pd concentrations were in the range of 0.095–2.86 wt%, which corresponded to a recovery of 94–97%.

$$Pd^{2+} + Fe^0 \rightarrow Pd^0 + Fe^{2+} \quad (1)$$

2.4. Dechlorination of PCE by Pd–Fe/SiO_2 microspheres

The dechlorination of PCE by mesoporous Pd–Fe/SiO_2 microspheres was performed by using batch experimental systems. N_2-purged serum bottles containing 0.1 g of Pd–Fe/SiO_2 or pure NZVI were filled with 50 mL of 25 mM HEPES buffer solution at pH 7.2 in a glove box. After being capped with Teflon-lined rubber septa and aluminium caps, the stock solutions of PCE were introduced into the bottles to get the final concentration of 5 mg L^{-1}. The serum bottles were then incubated in an orbital

 This journal is © The Royal Society of Chemistry 2015

Published on 09 October 2015. Downloaded by Gazi Universitesi on 09/03/2016 01:28:36.

shaker at 120 rpm and at 25 °C in the dark. Control experiments were also performed in the absence of the mesoporous Pd–Fe/SiO_2 microspheres.

The column experiments were performed by using a 15 mL glass burette packed with 0.4–0.6 mm glass beads to investigate the mobility and water permeability of the Pd–Fe/SiO_2 microspheres and NZVI. The column diameter was 1.5 cm and the total pore volume was 11.9 cm^3. The columns were saturated with deoxygenated deionized water before the addition of 2 g L^{-1} NZVI or Pd–Fe/SiO_2 suspensions. The flow rate of the feeding solution was 4.8 mL min^{-1}.

2.5. Analysis and characterization

The chlorinated as well as non-chlorinated hydrocarbons were determined by injecting 40 μL of headspace gas from the serum bottles into a Perkin-Elmer gas chromatograph (GC) equipped with an electron capture detector (ECD) and a flame ionization detector (FID). A VOCOL fused-silica megabore capillary column was used to separate the chlorinated and non-chlorinated compounds by isothermally maintaining 120 °C and using ultra high purity nitrogen (>99.9995%) as the carrier gas. The temperatures of the ECD and FID were maintained at 325 and 250 °C, respectively. Blank controls were also performed to examine the possible loss of chlorinated compounds during the dechlorination periods. In addition, the aqueous concentrations of chlorinated hydrocarbons were calculated using the external standard method by preparing known concentrations of chlorinated hydrocarbons in aqueous solutions.

The crystallite size and crystal phase of the Pd–Fe/SiO_2 microspheres were examined using a Scintag X1 advanced X-ray diffractometer (XRD) with Ni-filtered Cu Kα radiation (λ = 0.1541 nm). The XRD patterns were obtained from 20° to 70° 2θ with a sampling step width of 0.05° and a step time of 0.5 s. The specific surface area, pore volume and pore size distribution were determined by the N_2 adsorption–desorption isotherms at 77 K using a ASAP 2020 surface area and porosimetry system manufactured by Micromeritics Co. The Brunauer–Emmett–Teller (BET) method was utilized to calculate the specific surface areas (S_{BET}) using the adsorption data in a relative pressure (P/P_0) range from 0.02 to 0.2. By using the Barrett–Joyner–Halenda (BJH) model, the pore volumes and pore size distributions in the mesopore range (>2 nm) could be derived from the adsorption branches of the isotherms, and the total pore volumes (V_t) were calculated from the adsorbed amount at a relative pressure of 0.995.

The surface morphology of the mesoporous Pd–Fe/SiO_2 microspheres was observed using a JOEL field-emission scanning electron microscope (FE-SEM). The TEM images and particle sizes of Pd–Fe/SiO_2 were obtained using a Hitachi H-7500 transmission electron microscope at an acceleration voltage of 80 kV by suspending one drop of the microsphere suspension on a 300-mesh carbon coated Cu grid. The X-ray photoelectron spectroscopic (XPS) measurements were performed on a ESCA PHI 1600 photoelectron spectrometer using an Al Kα X-ray source (1486.6 eV). The binding energies of the photoelectrons were determined by assuming that the carbon 1s electron has a binding energy of 284.8 eV. During the data acquisition, the pressure in the sample chamber did not exceed 2.5×10^{-9} Torr.

3. Results and discussion

3.1. Microstructures of Fe/SiO_2 microspheres

The morphology and specific surface area of the mesoporous SiO_2 microspheres were first characterized. Fig. S1 (ESI†) shows the TEM images of mesoporous SiO_2 fabricated at various hydrothermal times ranging from 1 to 7 d. It is clear that the particle sizes of mesoporous SiO_2 increased with the increase in hydrothermal time and the particle diameters were in the range of 1–5 μm. In addition, the mesoporous silica showed typical type IV isotherms with a hysteresis loop in the P/P_0 range of 0.5–0.95, clearly showing the mesoporous characteristics of SiO_2 (Fig. S2, ESI†). The specific surface area of the mesoporous SiO_2 microspheres decreased from 312 $m^2 g^{-1}$ at 1 d to 164 $m^2 g^{-1}$ at 7 d, while the average pore diameter increased slightly from 6.9 to 8.6 nm when the hydrothermal time increased from 1 to 7 d. Since the role of the mesoporous SiO_2 microspheres used in this study is to serve as a support, the hydrothermal time of 1 d was selected because of the high surface area and similar pore diameter for the immobilization of NZVI.

Fig. 1 shows the SEM and TEM images of 10–50 wt% Fe/SiO_2 prepared by adding 50 mL of 0.2 M $NaBH_4$ into the mesoporous

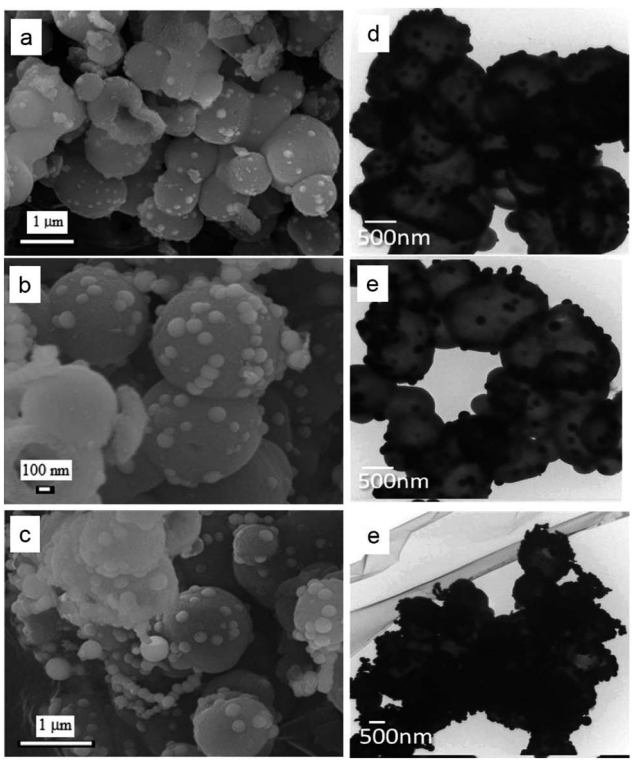

Fig. 1 The SEM and TEM images of various iron loadings of Fe/SiO_2 microspheres. (a–c) SEM images of 10, 30, and 50 wt% Fe/SiO_2, (d–f) TEM image of 10, 30 and 50 wt% Fe/SiO_2.

Published on 09 October 2015. Downloaded by Gazi Universitesi on 09/03/2016 01:28:36.

SiO_2 solutions containing ferrous ions. It is clear that the particle number as well as the size of the NZVI on the SiO_2 microspheres increased with the increase in Fe loading. No obvious aggregation of NZVI was observed when the loading of Fe was lower than 30 wt% (Fig. 1a and b). However, the NZVI aggregated into large particles at 50 wt% Fe and some NZVI nanoparticles were agglomerated into long chains outside of the SiO_2 microspheres (Fig. 1c). The EDS analysis indicated that the atomic ratios of Fe to Si were 0.122 for 10 wt% Fe/SiO_2, 0.316 for 30 wt% Fe/SiO_2 and 0.575 for 50 wt% Fe/SiO_2. In addition, the ICP-MS analysis showed similar results and the Fe concentration was 12.5 wt% for 10 wt% Fe/SiO_2, 30.3 wt% for 30 wt% Fe/SiO_2, and 45.1 wt% for 50 wt% Fe/SiO_2. These results clearly indicate the nearly complete reduction of ferrous ions to NZVI on the surface of mesoporous SiO_2 by $NaBH_4$.

Similar to the SEM images, the TEM images clearly showed the formation of discrete NZVI nanoparticles on the surface of the mesoporous SiO_2 microspheres when the Fe loadings were in the range 10–30 wt% (Fig. 1d and e). In contrast, the agglomeration of long-chained NZVI was clearly observed at 50 wt% Fe/SiO_2 (Fig. 1f). Fig. 2 shows a histogram of the particle sizes of NZVI on Fe/SiO_2 at various iron loadings of 10–50 wt%. The particle size distribution of NZVI at 10 wt% Fe/SiO_2 was in the range of 60–160 nm, and then increased to 120–240 nm at 50 wt% Fe/SiO_2. In addition, the average particle sizes of NZVI were 85 ± 27 nm, 150 ± 21 nm and 165 ± 30 nm for 10, 30, and 50 wt% Fe/SiO_2, respectively. No obvious difference in the mean diameter of NZVI between 30 and 50 wt% Fe/SiO_2 reflected the fact that 30 wt% could be the optimal iron loading for the mesoporous SiO_2 microspheres.

Fig. 3 shows the XRD patterns and specific surface areas of the Fe/SiO_2 microspheres with various Fe loading. As shown in Fig. 3a, the XRD pattern of pure NZVI showed peaks centered at 44.6° and 65.0° 2θ, which can be assigned to the (110) and (200) planes of body-centered cubic Fe (JCPDS 06-0696) respectively.[35] The broad peak at 20–25° 2θ for the Fe/SiO_2 microspheres was mainly attributed to the amorphous characteristics of SiO_2. In addition, the small and broad peak at 44.6° 2θ appeared when

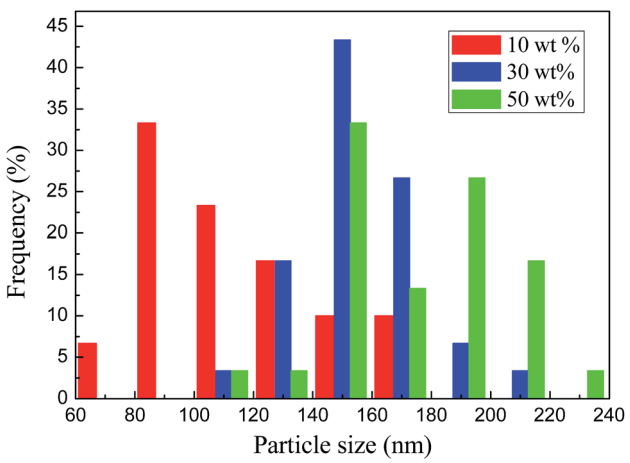

Fig. 2 The particle size distribution of NZVI on the Fe/SiO_2 microspheres at various iron loadings ranging from 10 to 50 wt%.

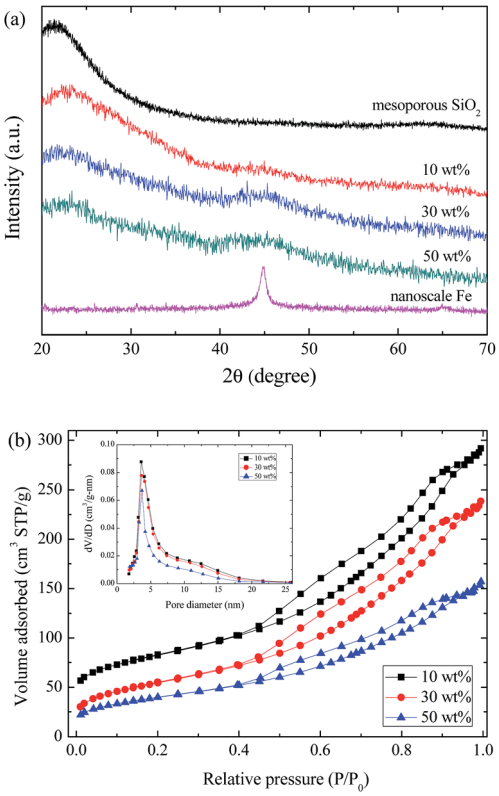

Fig. 3 The (a) XRD patterns and (b) N_2 adsorption–desorption isotherms of 10–50 wt% Fe/SiO_2. The insert in (b) is the pore size distribution of Fe/SiO_2. The *y*-axis of 10 wt% Fe/SiO_2 was vertically shifted by 25 $cm^3\ g^{-1}$ for clarity.

the iron loading increased from 10 to 50 wt%, indicating the successful immobilization of NZVI onto the surface of SiO_2.

Fig. 3b shows the BET surface area of the 10–50 wt% Fe/SiO_2 microspheres. Similar to the pure mesoporous SiO_2 microspheres, the N_2 adsorption–desorption isotherms of Fe/SiO_2 with varying Fe loadings followed a type IV physisorption isotherm with a H3 hysteresis loop in the P/P_0 range of 0.4–0.95, which is mainly attributed to capillary condensation in the mesopores of the silica substrate.[36] The specific surface areas of 10 and 30 wt% Fe/SiO_2 were in the range of 196–209 $m^2\ g^{-1}$ and then decreased to 143 $m^2\ g^{-1}$ when the Fe loading increased to 50 wt%. In addition, the pore size distributions of 10–50 wt% Fe/SiO_2 were similar and the average pore diameters were in the range of 5.7–6.0 nm, which indicate that the decrease in the specific surface area of 50 wt% Fe/SiO_2 is mainly attributed to the formation of large and excess NZVI nanoparticles onto and outside of the mesoporous SiO_2 microspheres. It is noteworthy that the average pore diameter of the Fe/SiO_2 microspheres is smaller than that of the pure SiO_2 microspheres, presumably attributed to the formation of NZVI on the surface of SiO_2 microspheres.

3.2. Microstructures of Pd–Fe/SiO_2 nanoparticles

After the successful fabrication of Fe/SiO_2, the Pd precursor was added to Fe/SiO_2 for the electrochemical formation of

 This journal is © The Royal Society of Chemistry 2015

Published on 09 October 2015. Downloaded by Gazi Universitesi on 09/03/2016 01:28:36.

bimetallic Pd–Fe nanoparticles on the mesoporous SiO_2 microspheres. The 30 wt% Fe/SiO_2 microspheres were selected as the support because of the homogenous Fe nanoparticles on the SiO_2 surface and the large specific surface area. Fig. S3 (ESI†) shows the XRD patterns of the 0.5–3 wt% Pd–Fe nanoparticles on the mesoporous SiO_2 microspheres. The XRD patterns of the Pd–Fe/SiO_2 microspheres (with various Pd loadings) showed broad peaks at 20–25° 2θ, which were similar to the results obtained by the Fe/SiO_2 microspheres. No Fe peak at 44.6° 2θ was observed, presumably attributed to the transformation of NZVI into iron oxides by providing electrons to electrochemically reduce Pd^{2+} into Pd^0. The TEM images of the 1–3 wt% Pd–Fe/SiO_2 microspheres clearly showed the formation of a thin layer on the surface of the NZVI with some needle-like structures (Fig. S4, ESI†), indicating the formation of iron oxides after the addition of the Pd ions. However, no characteristic Pd peak was observed because of the low amount of Pd added onto Fe/SiO_2.

To further elucidate the immobilization of Pd onto the Fe/SiO_2 surfaces, XPS was used to characterize the change in the chemical species of the elements in the Pd–Fe/SiO_2 microspheres. Fig. 4 shows the XPS spectra of the Si 2p, Fe 2p and Pd 3d species in the 3 wt% Pd–Fe/SiO_2 microspheres. The XP spectrum of Si 2p showed a broad peak at 100–105 eV, indicating the formation of SiO_2 (Fig. 4a). After Ar sputtering for 1 min to remove the top 27 nm of the particle surface, the Si 2p peak still remained at the same position, indicating the stability of SiO_2 as the support. The XPS of Fe 2p showed two peaks centered at 711 and 724 eV, which were the characteristic Fe $2p_{3/2}$ and Fe $2p_{1/2}$ peaks of iron oxides (Fig. 4b). Additional zerovalent iron peaks at 707 and 720 eV appeared after Ar sputtering for 1 min, clearly indicating the transformation of ZNVI to iron oxides after the addition of Pd^{2+}. This result also supports the XRD results, that no iron species was identified in the Pd–Fe/SiO_2 microspheres. In addition, the XPS peak of the iron oxides shifted from 711.8 eV to 710.4 eV. After peak deconvolution, the major species of the iron oxides changed from goethite (FeOOH) to magnetite (Fe_3O_4) after Ar sputtering (Fig. S5, ESI†), which reflected the fact that the reduction of Pd^{2+} to Pd^0 changed the species of the iron oxides on the surface of NZVI. The XPS spectra of the 3 wt% Pd loaded Fe/SiO_2 showed Pd 3d peaks at 334.9 and 340.2 eV, which belonged to Pd^0 $3d_{5/2}$ and Pd^0 $3d_{3/2}$, respectively (Fig. 4c). The peak positions of the Pd species did not change after Ar sputtering for 1 min, clearly indicating the formation of zerovalent Pd. In addition, no other peak related to the oxidation state of Pd^{2+} was observed, confirming the complete reduction of the immobilized Pd^{2+} to Pd^0 through the electrochemical Pd^{2+}–Fe^0 reduction reaction.

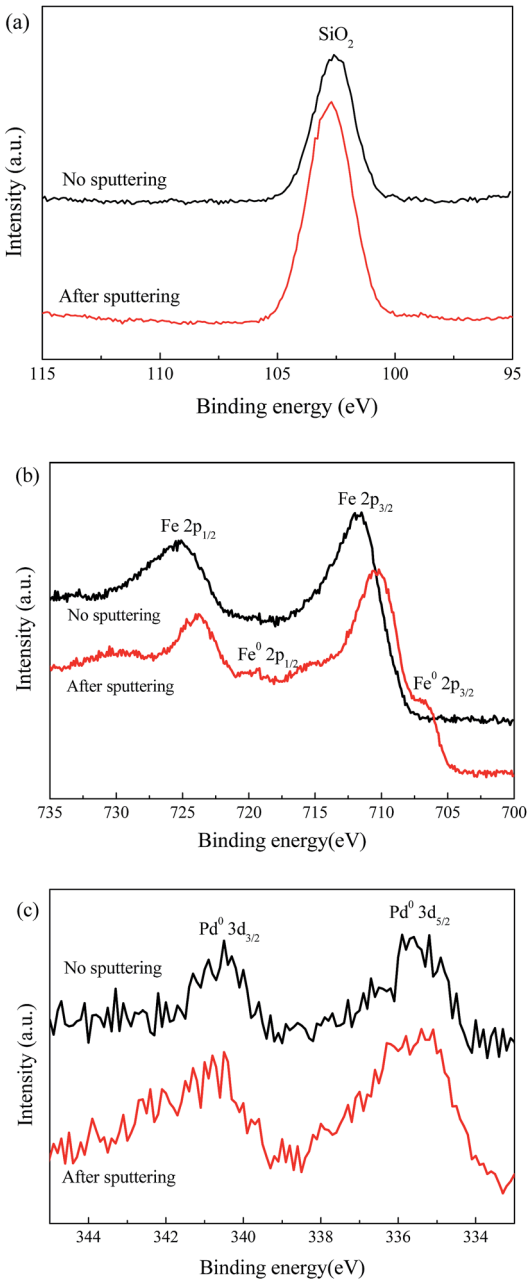

Fig. 4 The XPS spectra at (a) Si 2p, (b) Fe 2p and (c) Pd 3d of 3 wt% Pd–Fe/SiO_2 microspheres.

3.3. Dechlorination of PCE by Pd–Fe/SiO_2 microspheres

Since the SiO_2 microspheres are mesoporous materials and can adsorb organic contaminants, the adsorption of PCE by the mesoporous SiO_2 microspheres was examined first. Fig. S6 (ESI†) shows the adsorption of 5 mg L^{-1} PCE onto the mesoporous SiO_2 microspheres. No obvious decrease in the PCE concentration was observed after 50 h of incubation, indicating that the adsorption of PCE onto the mesoporous SiO_2 microspheres can be neglected. In addition, the PCE dechlorination efficiency of pure NZVI and Fe/SiO_2 was compared at pH 5.5. As shown in Fig. S7 (ESI†), the PCE dechlorination efficiency of Fe/SiO_2 after 575 h of incubation was higher than that of pure NZVI. The dechlorination followed pseudo-first-order rate kinetics and the pseudo-first-order rate constants (k_{obs}) for PCE dechlorination were 0.0061 and 0.0042 h^{-1} for the Fe/SiO_2 microspheres and pure NZVI, respectively. Since SiO_2 has no reactivity in PCE dechlorination, the dechlorination of PCE is mainly contributed by the NZVI on the SiO_2 microspheres and the rate constant for PCE dechlorination can be normalized to

Published on 09 October 2015. Downloaded by Gazi Universitesi on 09/03/2016 01:28:36.

the unit mass of NZVI to reflect the reactivity of NZVI on the Fe/SiO_2. After normalization to the unit mass of NZVI, the mass-normalized rate constant (k_m) for PCE dechlorination by Fe/SiO_2 was 0.01 L h^{-1} g^{-1}. This value is 4.8 times higher than that by pure NZVI, presumably attributed to the well-dispersed NZVI on the surface of the SiO_2 microspheres.

The addition of second catalytic metal ions such as Pd, Ni and Pt onto the iron surface can significantly enhance the dechlorination efficiency and dechlorination rate of chlorinated compounds.[35,37,38] Fig. 5a shows the PCE dechlorination efficiency of SiO_2-supported Pd–Fe nanoparticles at various Pd loadings of 0.1–3 wt%. The PCE dechlorination efficiency of Pd–Fe/SiO_2 increased significantly from 33% at 0.1 wt% Pd to 99.5% at 0.3 wt% Pd and nearly complete PCE dechlorination was observed with Pd loadings >0.5 wt%. Fig. 5b shows the k_{obs} for PCE dechlorination as a function of Pd loading. The k_{obs} values increased positively from 0.011 ± 0.004 min^{-1} at 0.1 wt% Pd to 0.267 ± 0.021 min^{-1} at 0.5 wt% Pd and then slightly decreased to 0.253 ± 0.023 min^{-1} when the Pd concentration increased to 3 wt%. These values are 2–3 orders of magnitude (108–2625 times) higher than that of the pure Fe/SiO_2 microspheres at pH 5.5, showing that the addition of low amounts of Pd ions can significantly enhance the dechlorination efficiency and dechlorination rate of PCE by mesoporous SiO_2-supported NZVI.

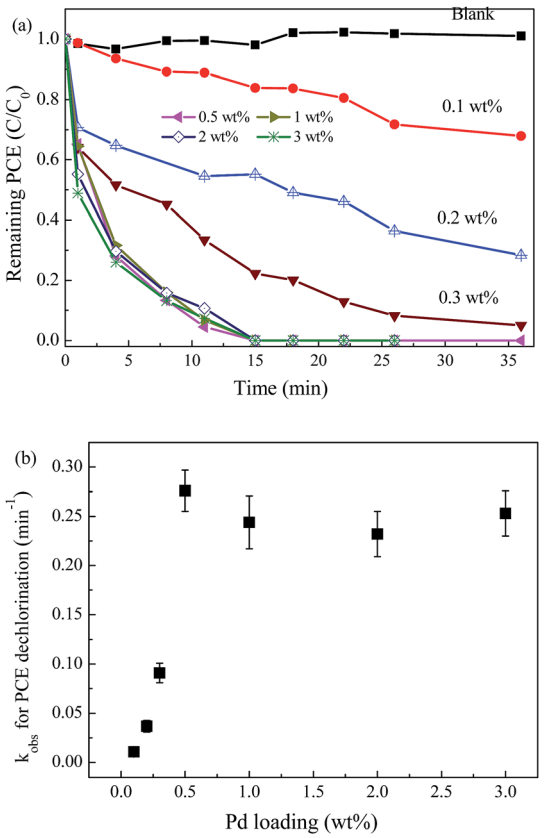

Fig. 5 (a) The dechlorination of PCE by 0.1–3 wt% Pd–Fe/SiO_2 under anoxic conditions and (b) pseudo-first-order rate constant for PCE dechlorination as a function of Pd loading.

Several studies have addressed the effect of additive loadings on the dechlorination efficiency of zerovalent metals toward chlorinated hydrocarbons.[39–41] An optimal mass loading often exists for a wide variety of bimetallic catalysts including Ni/Fe, Pd/Fe, Ni/Si and Ru/Fe. Lin *et al.* reported that the dechlorination rate of TCE by bimetallic Ru/Fe increased as the Ru loading increased from 0.25 to 1.5 wt%.[41] A decrease in k_{obs} was also observed when the Ru loading increased to 2.0 wt%. In this study, an optimal dosage of 0.5 wt% Pd ions was obtained for the dechlorination of PCE by the Fe/SiO_2 microspheres. The addition of catalytic Pd ions prevents the formation of toxic products by the dechlorination of chlorinated hydrocarbons *via* hydrogen reduction rather than through electron transfer.[35] As shown in Fig. 6, ethane was the only detected product for the dechlorination of PCE by 0.5–3 wt% Pd–Fe/SiO_2 and the carbon mass balances were all greater than 95%, showing that hydrodechlorination is the major reaction mechanism for the dechlorination of PCE by the mesoporous Pd–Fe/SiO_2 microspheres. In addition, several studies have reported the hydrodechlorination of gaseous PCE over Pd-based catalysts in the presence of hydrogen under high temperature conditions.[42–44] Bueres *et al.* immobilized 1 wt% Pd catalysts on three different carbonaceous materials and found that 68–97% of the gaseous PCE was converted to ethane and trace amounts of TCE by the carbon supported Pd at 525 K after 30 h of incubation.[44] This indicates that Pd only can show its dechlorination ability at high temperature and the Pd–Fe/SiO_2 microspheres are excellent catalysts for the hydrodechlorination of PCE in aqueous solutions.

The long-term performance of 0.5 wt% Pd–Fe/SiO_2 in the dechlorination of PCE was further investigated by repeatedly injecting 5 mg L^{-1} PCE into the solution containing Pd–Fe/SiO_2 microspheres. Fig. 7 shows the stability and longevity of Pd–Fe/SiO_2 with the repeated spiking of PCE under anoxic conditions. A fast PCE dechlorination process was observed and the Pd–Fe/SiO_2 microspheres can be reused for at least 10 times, all with

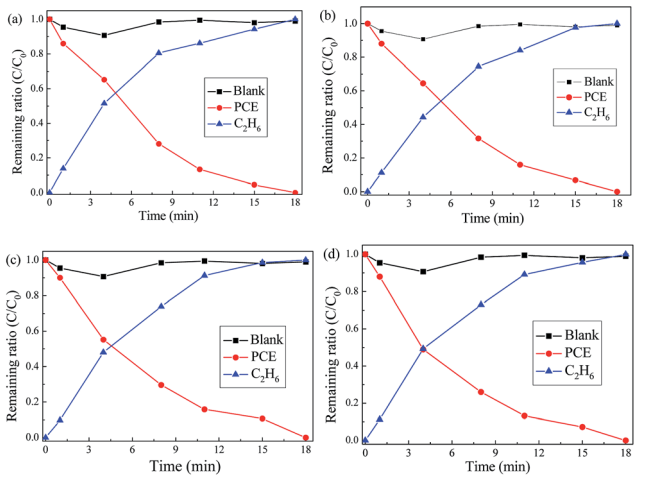

Fig. 6 The production of ethane and carbon mass balance during the dechlorination of PCE by the Pd–Fe/SiO_2 microspheres (various Pd loadings). (a) 0.5, (b) 1, (c) 2 and (d) 3 wt% Pd.

This journal is © The Royal Society of Chemistry 2015

Published on 09 October 2015. Downloaded by Gazi Universitesi on 09/03/2016 01:28:36.

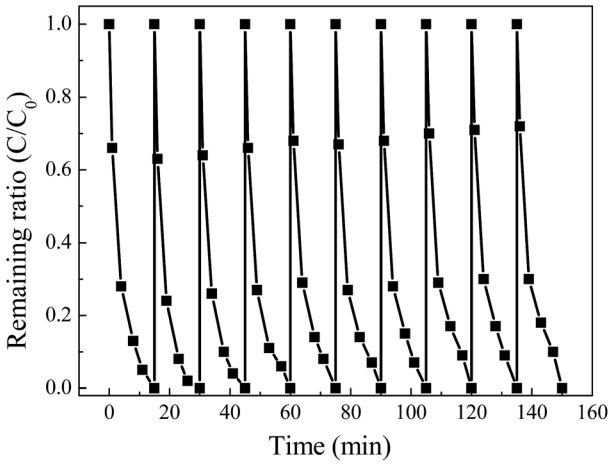

Fig. 7 The stability and longevity of mesoporous Pd–Fe/SiO_2 microspheres with repeated spiking of 5 mg L^{-1} PCE.

a stable dechlorination efficiency of >99%. Several studies have reported the repeated use of Pd/Fe nanoparticles for dechlorination. Nagpal *et al.* have used bimetallic Fe–Pd nanoparticles for lindane degradation under anoxic conditions and found that the dechlorination efficiency of the recycled Fe–Pd dropped slightly to 92% after the 10^{th} cycle.[45] In this study, the k_{obs} values and initial rate for PCE dechlorination were in the range 0.207–0.271 min^{-1} and 8.96–11.5 μM min^{-1}, respectively, showing that the 0.5 wt% Pd–Fe/SiO_2 microspheres are a promising material for the dechlorination of chlorinated hydrocarbons. The stability of Pd–Fe/SiO_2 is mainly attributed to the introduction of SiO_2 as the support. Reardon *et al.* have proposed that the presence of silica may slow down iron corrosion by adsorbing silicate, the dissolved form of SiO_2 after reaction, to the anodic surface.[46] In this study, the solution pH after dechlorination in the presence of the Fe/SiO_2 microspheres increased by 0.4–0.8 units which is lower than that in the presence of pure NZVI (1–1.5 units). This result supports the hypothesis that the introduction of the SiO_2 microspheres could maintain the reactivity of NZVI with >99% dechlorination efficiency of PCE.

3.4. Column experiments

One of the advantages of using mesoporous SiO_2 microspheres as the support is the high mobility and water permeability during the dechlorination processes. To prove the merits of mesoporous SiO_2 microspheres, column experiments were conducted to understand the water permeability in the presence of the Pd–Fe/SiO_2 microspheres. As shown in Fig. S8 (ESI†), pure NZVI was retained at the top of the column, which was similar to reported data.[22,47] In contrast, the Pd–Fe/SiO_2 microspheres could transport along with the water through the whole column, which indicates the good transportability of Pd–Fe/SiO_2. Fig. 8 shows the breakthrough curves of pure NZVI and Pd–Fe/SiO_2. It is clear that the mass ratios of pure NZVI in the effluent were in the range of 0.01–0.06 in the first 6 pore volumes, showing that NZVI would be aggregated into large particles and then retained

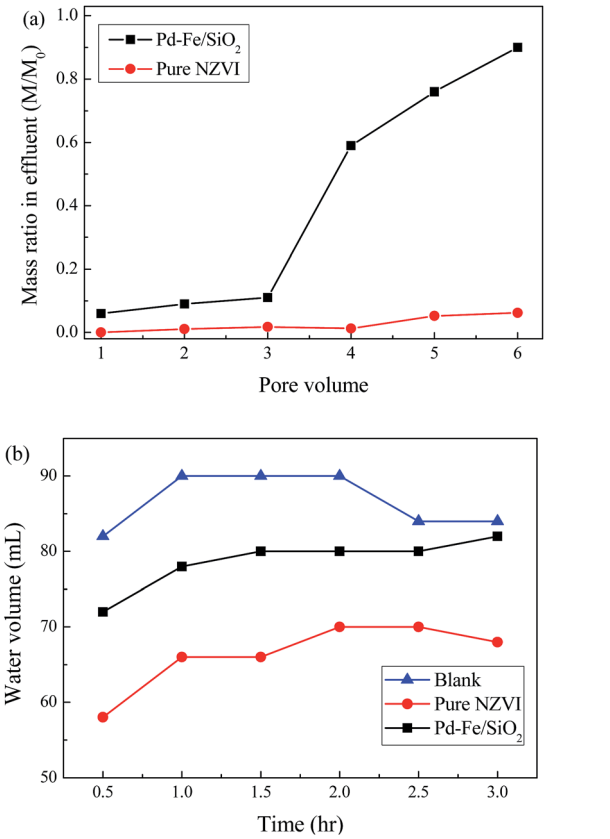

Fig. 8 (a) The breakthrough curves and (b) permeability of pure NZVI and mesoporous 0.5 wt% Pd–Fe/SiO_2 microspheres. M/M_0 represents the fraction of particles that are eluted in the effluent.

in the column. On the contrary, the mass of the Pd–Fe/SiO_2 microspheres in the effluent started to increase after 3 pore volumes and 90% of Pd–Fe/SiO_2 was eluted from the column after 6 pore volumes. Zhan *et al.* compared the mobility of Fe/ethylsilica and NZVI using a column packed with standard Ottawa sand and found that most NZVI was trapped within the first few centimeters of the column, while the Fe/ethylsilica particles reached the bottom of the column,[47] which is consistent with the results obtained in this study.

Fig. 8b shows the water permeability of pure NZVI and Pd–Fe/SiO_2 by packing 1 cm of different materials in the middle of the column. In the absence of Fe-based particles, the average water flow in the glass bead packed column was 82–90 mL h^{-1}, and slightly decreased to 72–80 mL h^{-1} in the presence of the mesoporous Pd–Fe/SiO_2 microspheres. However, the water flow decreased to 58–70 mL h^{-1} when pure NZVI was packed in the column, showing that the mesoporous SiO_2 microspheres are a good support with good permeability to disperse NZVI for the remediation of chlorinated compounds in porous media.

Fig. 9 shows the possible reaction mechanism for PCE dechlorination by the mesoporous Pd–Fe/SiO_2 microspheres under anoxic conditions. The negatively charged silica surface can adsorb Fe^{2+} ions and then convert them to NZVI in the presence of $NaBH_4$, which can be well dispersed on the surface of the SiO_2 microspheres to enhance the reactivity of Fe/SiO_2.

Published on 09 October 2015. Downloaded by Gazi Universitesi on 09/03/2016 01:28:36.

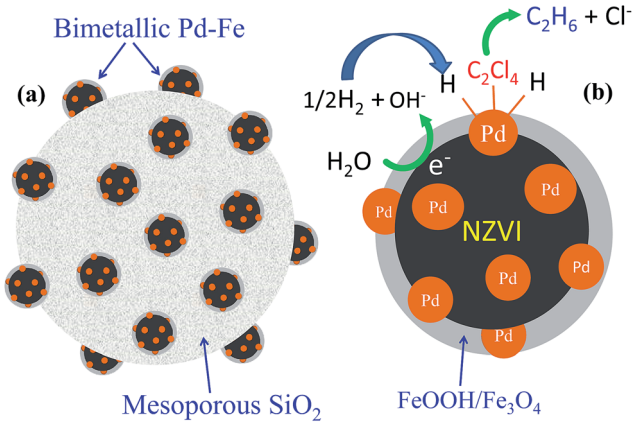

Fig. 9 The (a) immobilization of Pd–Fe nanoparticles onto mesoporous SiO_2 microspheres and (b) proposed mechanism for PCE dechlorination by mesoporous Pd–Fe/SiO_2 microspheres.

The silica-supported Pd–Fe nanoparticles were electrochemically generated when the Pd^{2+} ions were adsorbed onto the NZVI surfaces. The hydrodechlorination of PCE by the bimetallic Pd–Fe nanoparticles involves the oxidation of NZVI to galvanically protect the Pd metal and the Pd metal provides active sites for hydrodechlorination.[48] As the corrosion of NZVI increases, protons from water are reduced to adsorbed H atoms and to molecular hydrogen at the catalytic Pd surface, resulting in the formation of ethane during the hydrodechlorination of PCE.

4. Conclusions

In this study, we have first demonstrated the use of mesoporous SiO_2 microspheres as a support to well disperse bimetallic Pd–Fe nanoparticles for the hydrodechlorination of PCE under anoxic conditions. TEM images and surface area analysis showed that the poorly crystalline SiO_2 provided large specific surface areas for the immobilization of Pd–Fe nanoparticles. The dechlorination reaction by Fe/SiO_2 followed a pseudo-first-order reaction and the Fe mass normalized rate constant of Fe/SiO_2 was 5.2 times higher than that of pure NZVI at pH 5.5. The addition of Pd ions enhanced the efficiency and dechlorination rate and the k_{obs} for PCE dechlorination by Fe/SiO_2 was significantly enhanced by 2–3 orders of magnitude after the addition of 0.5–3 wt% Pd ions. The Pd–Fe/SiO_2 microspheres showed excellent reusability for PCE dechlorination, and they can be recycled at least 10 times. The mesoporous silica plays an important role in immobilizing and well dispersing NZVI on the surface, which can provide the maximum number of active sites for the dechlorination of PCE. The column experiments prove that mesoporous silica is a good carrier for bimetallic Pd–Fe nanoparticles; to pass through the bed of glass beads and helping them have better permeability than bare NZVI. The results obtained in this study clearly indicate that the mesoporous Pd–Fe/SiO_2 microspheres are environmentally friendly composites for the effective and efficient dechlorination of chlorinated hydrocarbons and can open an avenue to tailor mesoporous nanocomposites for the long-term dechlorination of chlorinated compounds in porous media.

Acknowledgements

The authors thank the Ministry of Science and Technology (MOST), Taiwan for financial support under grant No. NSC 101-2221-E-007-084-MY3.

Notes and references

1 D. Kaown, O. Shouakar-Stash, J. Yang, Y. Hyun and K. K. Lee, *Groundwater*, 2014, **52**, 875–885.
2 M. Muchitsch, T. van Nooten, L. Bastiaens and P. Kjeldsen, *J. Contam. Hydrol.*, 2011, **126**, 258–270.
3 J. E. Cambers, M. H. Loke, R. D. Ogilvy and P. I. Meldrum, *J. Contam. Hydrol.*, 2004, **68**, 1–22.
4 J. Koenig, M. Lee and M. Manefield, *Rev. Environ. Sci. Bio/Technol.*, 2015, **14**, 49–71.
5 I. Bacsi, S. Gonda, V. B-Beres, Z. Novak, S. A. Nagy and G. Vasas, *Ecotoxicology*, 2015, **24**, 823–834.
6 J. Z. Zheng, Z. J. Xue, S. F. Li, S. X. Li and Z. M. Rao, *Anal. Methods*, 2012, **4**, 2791–2796.
7 R. A. Doong, C. C. Lee and C. M. Lien, *Chemosphere*, 2014, **97**, 54–63.
8 Y. Ma, X. M. Du, Y. Shi, Z. Xu, J. D. Fang, Z. Li and F. S. Li, *Chemosphere*, 2015, **121**, 117–123.
9 R. A. Maithreepala and R. A. Doong, *Environ. Sci. Technol.*, 2005, **39**, 4082–4090.
10 X. Liang, Y. Dong, T. Kuder, L. R. Krumholz, R. P. Philp and E. C. Bulter, *Environ. Sci. Technol.*, 2007, **41**, 7094–7100.
11 C. C. Lee and R. A. Doong, *Appl. Catal., B*, 2014, **144**, 182–188.
12 F. L. Fu, D. D. Dionysiou and H. Liu, *J. Hazard. Mater.*, 2014, **267**, 194–205.
13 C. C. Huang and H. L. Lien, *Water Sci. Technol.*, 2010, **62**, 202–208.
14 G. K. Parshetti and R. A. Doong, *Chemosphere*, 2012, **86**, 392–399.
15 N. C. Mueller, J. Braun, J. Bruns, M. Černík, P. Rissing, D. Rickerby and B. Nowack, *Environ. Sci. Pollut. Res.*, 2012, **19**, 550–558.
16 W. Yan, H. L. Lien, B. E. Koelc and W. X. Zhang, *Environ. Sci.: Processes Impacts*, 2013, **15**, 63–77.
17 Y. H. Shih, M. Y. Chen and Y. F. Su, *Appl. Catal., B*, 2011, **105**, 24–29.
18 H. L. Lien and W. X. Zhang, *Appl. Catal., B*, 2007, **77**, 110–116.
19 R. A. Doong and Y. L. Lai, *Chemosphere*, 2006, **64**, 371–378.
20 F. He, D. Y. Zhao and C. Paul, *Water Res.*, 2010, **44**, 2360–2370.
21 P. Jiemvarangkul, W. X. Zhang and H.-L. Lien, *Chem. Eng. J.*, 2011, **170**, 482–491.
22 C. M. Kocur, A. I. Chowdhury, N. Sakulchaicharoen, H. K. Boparai, K. P. Weber, P. Sharma, M. M. Krol, L. Austrins, C. Peace, B. E. Sleep and D. M. O'Carroll, *Environ. Sci. Technol.*, 2014, **48**, 2862–2869.

This journal is © The Royal Society of Chemistry 2015

Published on 09 October 2015. Downloaded by Gazi Universitesi on 09/03/2016 01:28:36.

23 H. Ma, Y. P. Huang, M. W. Shen, R. Guo, X. Y. Cao and X. Y. Shi, *J. Hazard. Mater.*, 2012, **11–212**, 349–356.
24 F. He and D. Y. Zhao, *Environ. Sci. Technol.*, 2007, **41**, 6216–6221.
25 B. Schrick, B. W. Hydutsky, J. L. Blough and T. E. Mallouk, *Chem. Mater.*, 2004, **16**, 2187–2193.
26 V. Smuleac, R. Varma, S. Sikdar and D. Bhattacharyya, *J. Membr. Sci.*, 2011, **379**, 131–137.
27 Y. F. Su, T. L. Cheng and Y. S. Shih, *J. Environ. Manage.*, 2013, **129**, 361–366.
28 G. K. Parshetti and R. A. Doong, *Water Res.*, 2009, **43**, 3086–3094.
29 S. X. Li, J. Z. Zheng, D. J. Chen, Y. J. Wu, W. X. Zhang, F. Y. Zheng, J. Cao, H. Ma and Y. L. Liu, *Nanoscale*, 2013, **5**, 11718–11724.
30 C. H. Tan, W. X. Zhang, J. Z. Zheng, X. L. You, X. A. Lin and S. Z. Li, *J. Mater. Chem. B*, 2015, **3**, 7117–7124.
31 W. X. Xhang, J. Z. Zheng, X. H. Tan, C. H. Tan, X. A. Lin, S. R. Hu, J. H. Chen, X. L. You and S. X. Li, *J. Mater. Chem. B*, 2015, **3**, 217–224.
32 Y. Y. Xie, Z. Q. Fang, X. H. Qiu, E. P. K. Tsang and B. Liang, *Chemosphere*, 2014, **108**, 433–436.
33 L. M. Kustov, S. R. Al-Abed, J. Virkutyte, O. A. Kirichenko, E. V. Shuvalova, G. I. Kapustin, I. V. Mishin, V. D. Nissenbaum, O. P. Tkachenko and E. D. Finashina, *Pure Appl. Chem.*, 2014, **86**, 1141–1158.
34 B. Ensie and S. Samad, *Desalination*, 2014, **347**, 1–9.
35 P. X. Wu, C. M. Liu, Z. J. Huang and W. M. Wang, *RSC Adv.*, 2014, **4**, 25580–25587.
36 Q. Cai, Z. S. Luo, W. Q. Pang, Y. W. Fan, Z. H. Chen and F. Z. Cui, *Chem. Mater.*, 2001, **13**, 258–263.
37 L. Yang, L. Lv, S. Zhang, B. Pan and W. Zhang, *Chem. Eng. J.*, 2011, **178**, 161–167.
38 G. K. Parshetti and R. A. Doong, *Water Res.*, 2011, **45**, 4198–4210.
39 Y. H. Tee, E. Grulke and D. Bhattacharyya, *Ind. Eng. Chem. Res.*, 2005, **44**, 7062–7070.
40 C. C. Lee and R. A. Doong, *Environ. Sci. Technol.*, 2008, **42**, 4752–4757.
41 C. J. Lin, S. L. Lo and Y. H. Liou, *J. Hazard. Mater.*, 2004, **116**, 219–228.
42 C. A. González and C. M. de Correa, *Ind. Eng. Chem. Res.*, 2010, **49**, 490–497.
43 S. Pitkaaho, L. Matejova, S. Ojala, J. Gaalova and R. L. Keiski, *Appl. Catal., B*, 2012, **113–114**, 150–159.
44 R. F. Bueres, E. Asedegbega-Nieto, E. Díaz, S. Ordóñez and F. V. Díez, *Catal. Today*, 2010, **150**, 16–21.
45 V. Nagpal, A. D. Bokare, R. C. Chikate, C. V. Rode and K. M. Paknikar, *J. Hazard. Mater.*, 2010, **175**, 680–687.
46 E. J. Reardon, R. Fagan, J. L. Vogan and A. Przepiora, *Environ. Sci. Technol.*, 2008, **42**, 2420–2425.
47 J. J. Zhan, T. H. Zheng, G. Piringer, C. Day, G. L. McPherson, Y. F. Lu, K. Papadopoulos and V. T. John, *Environ. Sci. Technol.*, 2008, **42**, 4494–4499.
48 S. J. Li, Y. L. Fang, C. D. Romanczuk, Z. H. Jin, T. L. Li and M. S. Wong, *Appl. Catal., B*, 2012, **25**, 95–102.